UNIVERSIDAD DE CONCEPCIÓN

Centro de Investigación en Ingeniería Matemática (CI^{2}MA)

A degenerating convection-diffusion model of a flotation column: theory, numerics and applications

Fernando Betancourt, Raimund Bürger,
Stefan Diehl, María Carmen Martí,
Yolanda Vásquez

PREPRINT 2024-08

SERIE DE PRE-PUBLICACIONES

A DEGENERATING CONVECTION-DIFFUSION MODEL OF A FLOTATION COLUMN: THEORY, NUMERICS AND APPLICATIONS*

FERNANDO BETANCOURT[A], RAIMUND BÜRGER[B,**], STEFAN DIEHL[C], MARÍA DEL CARMEN MARTÍ[D], AND YOLANDA VÁSQUEZ[E]

Abstract. The operation of a froth flotation column can be described by a nonlinear convection-diffusion partial differential equation that incorporates the solids–flux and drift–flux theories as well as a model of foam drainage. The resulting model contains some non-standard ingredients such as discontinuous fluxes and degenerating diffusion accounting for foam drainage. It predicts the bubble and gangue particle volume fractions as functions of height and time. The steady-state (time-independent) version of the model defines so-called operating charts that map conditions on the gas and pulp feed rates that allow for operation with a stationary froth layer. In addition, a robust numerical scheme allows for the efficient simulation of the dynamic (transient) behaviour of the flotation column. Examples, in part for the addition of solid particles, are presented.

1. Introduction and research problem

Froth flotation is an important stage especially of copper mining in Chile. The flotation process selectively separates hydrophobic materials (that are repelled by water) from hydrophilic (that would be attracted to water), where both are suspended in a viscous fluid. It is well known that a flotation column works as follows: gas is introduced close to the bottom and generates bubbles that rise through the continuously injected pulp that contains the solid particles. The hydrophobic particles (the valuable mineral particles) attach to the rising bubbles, forming froth that is removed through a launder. The hydrophilic particles (slimes or gangue) do not attach to bubbles but settle to the bottom (unless they are trapped in the bulk upflow) and are removed continuously as flotation tailings. Close to the top, additional wash water can be injected to assist with the rejection of entrained impurities and increase froth stability (Pal and Masliyah, 1989; Finch and Dobby, 1990; Vandenberghe et al., 2005; Wills and Napier-Munn, 2006; Dunne et al., 2019; Concha and Bascur, 2024). This unit operation is particularly suitable for processing low-grade ores

Date: May 8, 2024.

Key words and phrases. Froth flotation; drainage; drift flux; mathematical model; partial differential equation; steady state; numerical simulation.

*Presented at the *11th International Flotation Conference (Flotation '23)*, Cape Town, South Africa, November 6–9, 2023, organized by Minerals Engineering International (MEI).

**Corresponding author.

[A]CI^{2}MA and Departamento de Ingeniería Metalúrgica, Facultad de Ingeniería, Universidad de Concepción, Casilla 160-C, Concepción, Chile. E-Mail: fbetancourt@udec.cl.

[B]CI^{2}MA and Departamento de Ingeniería Matemática, Facultad de Ciencias Físicas y Matemáticas, Universidad de Concepción, Casilla 160-C, Concepción, Chile. E-Mail: rburger@ing-mat.udec.cl.

[C]Centre for Mathematical Sciences, Lund University, P.O. Box 118, S-221 00 Lund, Sweden. E-Mail: stefan.diehl@math.lth.se.

[D]Departament de Matemàtiques, Universitat de València, Avda. Vicent Andrés Estellés s/n, E-46100 Burjassot, València, Spain. E-Mail: Maria.C.Marti@uv.es.

[E]Facultad de Ciencias y Tecnología, Universidad Tecnológica de Panamá, Panama. E-Mail: yolanda.vasquez@utp.ac.pa.

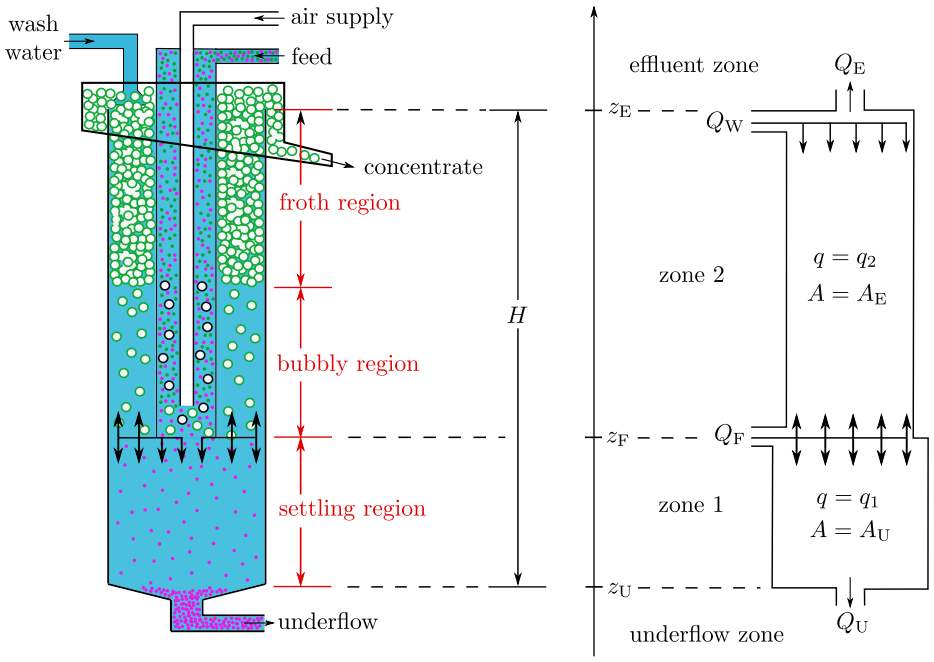

FIGURE 1. Left: Schematic of a flotation column; cf. the Reflux Flotation Cell by Dickinson and Galvin (2014). Right: The corresponding one-dimensional conceptual model with a non-constant cross-sectional area $A(z)$. Wash water is sprinkled at the effluent level $z = z_E$ and a mixture of aggregates and feed slurry is fed at $z = z_F$, where $z_U < z_F < z_E$ divide the real line into the zones inside the column and the underflow and effluent zones.

but requires huge amounts of process water. Since water is a scarce resource for most economic activity in Chile, in particular in the desert areas where most mines are located, the improvement of the scientific understanding of flotation processes and the development of tools for the design, simulation and control of flotation devices is of critical economical, ecological and societal importance. This situation has been motivating collaborative research between applied mathematicians and metallurgical engineers at Universidad de Concepción, jointly with collaborators from Panama, Spain and Sweden.

References to current research on modelling flotation and developing strategies for its control include Cruz (1996), Maldonado et al. (2009), Bergh and Yianatos (2011), Tian et al. (2018a,b), Azhin et al. (2021a,b), and Quintanilla et al. (2021a,b,c). The development of control strategies requires dynamic models along with a classification of steady-state (stationary) solutions. These models should focus on separation aligned with gravity, and therefore they are spatially one-dimensional. In fact, we wish to avoid the additional computational effort associated with spatially two- or three-dimensional models based on computational fluid dynamics (CFD) (but see Wang et al. (2018) for a review on CFD-based models). The sought unknowns are the volume fractions of gas (bubbles), liquid, and solid particles as functions of time and spatial position, so the resulting governing equations are partial differential equations (PDEs).

It is the purpose of this contribution to present a summary of recent research conducted by the authors (Betancourt et al., 2023; Bürger et al., 2019, 2020a, 2020b, 2022, 2023; Vásquez, 2022)

related to a PDE model formulated as a system of two nonlinear, scalar convection-diffusion equations (see below). The approach provides a complete model of the solids-gas-fluid hydrodynamics, including froth drainage, in a flotation column. Several variants of the setup have been considered in these works; we here refer to the one utilized by Bürger et al. (2022), see Figure 1. The novelty of the present work are new operating charts, steady-state computations and numerical simulations, and an analysis of the effect of varying the parameters of the drift-flux velocity function on the size, location, and shape of the desirable (feasible) steady-state region of an operating chart.

2. Related work

The final model incorporates several available (partial) theories, including the following:

- The drift-flux theory (Wallis, 1969) to describe the bubble velocity relative to the ambient mixture. With additional bulk flows due to the inlets and outlets of the column that theory has mostly been used for steady-state investigations of flotation columns (Vandenberghe et al., 2005; Stevenson et al., 2008; Dickinson and Galvin, 2014; Galvin and Dickinson, 2014; Galvin et al., 2014). In the current approach, it is part of the transient simulation model.
- The similar, established solids flux theory for sedimentation of gangue particles (Kynch, 1952; Diehl, 2001, 2008; Ekama and Marais, 2004).
- A one-dimensional formulation of available theories of drainage of froth due to capillarity, drainage, and dissipation that describes the variation of fluid volume fraction through the foam (Neethling et al., 2002; Neethling and Cilliers, 2003; Stevenson, 2006; Stevenson et al., 2008; Brito-Parada et al., 2012; Neethling and Brito-Parada, 2018).
- The description of a continuously operated column in one space dimension including singular source terms, discontinuous spatial variation of bulk flows, and replacement of boundary conditions through the principle of continuity of flux, akin to models of continuous sedimentation of flocculated suspensions in clarifier-thickeners (Diehl, 1996; Bürger et al., 2004, 2005).

3. Main results

The final model was chosen as a topic of study of mathematical and numerical analysis, and in particular gave rise to the last author's doctoral thesis (Vásquez, 2022). The main results from the viewpoint of applications are the following:

- The model describes the transient variation of bubble and solids concentrations as functions of height and time. A time-independent version describes steady-state solutions. Exploiting jump conditions (consequences of the principle of continuity of flux) and entropy conditions (arising from uniqueness issues), one may establish conditions for the existence of desirable bubble concentration profiles, in particular for the existence of a froth layer. These are algebraic conditions for the range of operating parameters (feed rates, wash water rates, and gas concentrations) that can conveniently be mapped as operating charts.
- In-house experiments with a laboratory flotation column indicate a narrow range of conditions for froth stability, in agreement with theoretical stability analysis.
- Analysis of the impact of varying the parameters of the drift-flux velocity function demonstrated significant modifications to the operating charts and adjustments to capillarity parameters were directly linked to changes in the froth layer, emphasizing the critical role of capillary forces in the system's dynamics.
- A robust numerical scheme to (approximately) solve the time-dependent model and simulate the transient operation of the flotation column. Numerically simulated concentrations

provably attain physically relevant values (volume fractions are nonnegative and sum up to one).

- The pulp-foam interface does not need to be tracked explicitly. Transient simulations with constant inputs converge to steady states predicted by the operating charts.

4. Mathematical model

The three phases and their (dimensionless) volume fractions are the fluid $\phi_\mathrm{f} = \phi_\mathrm{f}(z,t)$, the solids $\psi = \psi(z,t)$, and the bubbles (aggregates) $\phi = \phi(z,t)$, where $\phi_\mathrm{f} + \psi + \phi = 1$. A mixture of fluid and solid particles is addressed as suspension. The volume fraction of solids within the suspension that fills the interstices between bubbles φ is defined by

$$\varphi := \frac{\psi}{\psi + \phi_\mathrm{f}} = \frac{\psi}{1-\phi}.$$

In what follows, we provide the description for the column drawn in Figure 1, where the feed pulp and the gas are assumed to enter through the same feed inlet at $z = z_\mathrm{F}$ and the effluent height level $z = z_\mathrm{E}$ and that of injection of wash water $z = z_\mathrm{W}$ are identified ($z_\mathrm{E} = z_\mathrm{W}$). Thus, the interior of the flotation column can be subdivided into two zones (zones 1 and 2, see Figure 1). Variants of this setup can be handled by similar equations, for example when there is a separate gas inlet (Betancourt et al., 2023) or we consider a general model with an arbitrary number of feed inlets (Bürger et al., 2023); those configurations give rise to three or more zones.

The system of PDEs that governs the evolution of ϕ and ψ can be formulated as

$$\begin{aligned} A(z)\frac{\partial \phi}{\partial t} + \frac{\partial}{\partial z}\big(A(z)J(\phi,z,t)\big) &= \frac{\partial}{\partial z}\left(A(z)\gamma(z)\frac{\partial D(\phi)}{\partial z}\right) + Q_\mathrm{F}\phi_\mathrm{F}(t)\delta(z-z_\mathrm{F}), \\ A(z)\frac{\partial \psi}{\partial t} + \frac{\partial}{\partial z}\big(-A(z)\tilde{F}(\psi,\phi,z,t)\big) &= \frac{\partial}{\partial z}\left(A(z)\gamma(z)\frac{-\psi}{1-\phi}\frac{\partial D(\phi)}{\partial z}\right) + Q_\mathrm{F}\psi_\mathrm{F}(t)\delta(z-z_\mathrm{F}). \end{aligned} \tag{4.1}$$

Here $A = A(z)$ is the cross-sectional area of the tank, and $J = J(\phi,z,t)$ and $\tilde{F} = \tilde{F}(\psi,\phi,z,t)$ are convective flux functions that depend discontinuously on z at the feed inlet ($z = z_\mathrm{F}$), the underflow outlet ($z = z_\mathrm{U}$) at the bottom, and the overflow outlet ($z = z_\mathrm{E}$). The system (4.1) is valid for $t > 0$ and is solved with initial conditions. The function γ indicates the interior of the tank:

$$\gamma(z) := \begin{cases} 1 & \text{inside the tank, i.e., if } z_\mathrm{U} \le z \le z_\mathrm{E}, \\ 0 & \text{outside the tank, i.e., if } z < z_\mathrm{U} \text{ or } z > z_\mathrm{E}. \end{cases}$$

Moreover, the cross-sectional area is assumed to satisfy

$$A(z) = \begin{cases} A_\mathrm{E} & \text{for } z \ge z_\mathrm{F}, \\ A_\mathrm{F} & \text{for } z < z_\mathrm{F}; \end{cases}$$

we hereby take into account that part of the available total cross-sectional area of the column is occupied by the feed inlet for $z \ge z_\mathrm{F}$. The nonlinear function D models capillarity when bubbles are in contact and has the properties

$$D(\phi) := \int_0^\phi d(s)\,\mathrm{d}s, \quad \text{where} \quad d(\phi) = D'(\phi) \begin{cases} = 0 & \text{for } 0 \le \phi \le \phi_\mathrm{c}, \\ > 0 & \text{for } \phi_\mathrm{c} < \phi \le 1. \end{cases}$$

Here ϕ_c is a critical bubble volume fraction that marks the transition between pulp and froth. Consequently, at each point (z,t) where $\phi(z,t) \le \phi_\mathrm{c}$, there holds $D(\phi(z,t)) = 0$. The last term on the right-hand sides of (4.1) describes a singular source located at level $z = z_\mathrm{F}$, where $Q_\mathrm{F}(t)$ is the corresponding volume feed rate (as a given function of time) and $\phi_\mathrm{F}(t)$ and $\psi_\mathrm{F}(t)$ are the respective

bubble and solids feed concentrations. Outside the tank, the mixture is assumed to follow the outlet streams. Consequently, boundary conditions are not needed; conservation of mass determines the outlet volume fractions in a natural way.

Details of the fluxes and capillarity functions of (4.1) are now given. Applying the conservation of mass to each of the three phases, introducing the volume-average velocity, or bulk velocity, of the mixture q and the relative velocities of both the aggregate-suspension and the solid-fluid, one obtains the flow rates (velocities) in and out of the flotation column

$$q(z,t) := \begin{cases} q_{\mathrm{E}} := (-Q_{\mathrm{U}} + Q_{\mathrm{F}} + Q_{\mathrm{W}})/A & \text{in the effluent zone,} \\ q_2 := (-Q_{\mathrm{U}} + Q_{\mathrm{F}})/A & \text{in zone 2,} \\ q_1 = q_{\mathrm{U}} := -Q_{\mathrm{U}}/A_{\mathrm{U}} & \text{in zone 1 and the underflow.} \end{cases}$$

The drift-flux and solids-flux theories utilize constitutive functions for the aggregate upward batch flux $j_{\mathrm{b}}(\phi)$ and the solids batch sedimentation flux $f_{\mathrm{b}}(\varphi) := \varphi v_{\mathrm{hs}}(\varphi)$, where $v_{\mathrm{hs}}(\varphi)$ is the hindered-settling function. For simplicity, we use the well-known expression due to Richardson and Zaki (1954) $v_{\mathrm{hs}}(\varphi) = v_\infty(1-\varphi)^{n_{\mathrm{RZ}}}$, where $n_{\mathrm{RZ}} > 1$, and v_∞ is the velocity of a single particle. In the underflow and effluent, all phases are assumed to have the same velocity, i.e., they follow the bulk flow. Then the total convective fluxes for ϕ and φ are given by

$$J(\phi,z,t) = \begin{cases} j_{\mathrm{E}}(\phi,t) := q_{\mathrm{E}}(t)\phi & \text{in the effluent zone,} \\ j_2(\phi,t) := q_2(t)\phi + j_{\mathrm{b}}(\phi) & \text{in zone 2,} \\ j_1(\phi,t) := q_1(t)\phi + j_{\mathrm{b}}(\phi) & \text{in zone 1,} \\ j_{\mathrm{U}}(\phi,t) := q_1(t)\phi & \text{in the underflow zone,} \end{cases}$$

$$F(\varphi,\phi,z,t) = \begin{cases} f_{\mathrm{E}}(\varphi,\phi,t) := -(1-\phi)q_{\mathrm{E}}(t)\varphi & \text{in the effluent zone,} \\ f_2(\varphi,\phi,t) & \text{in zone 2,} \\ f_1(\varphi,\phi,t) & \text{in zone 1,} \\ f_{\mathrm{U}}(\varphi,\phi,t) := -(1-\phi)q_1(t)\varphi & \text{in the underflow zone,} \end{cases}$$

with the zone-settling flux functions (positive in the direction of sedimentation, that is, decreasing z)

$$\begin{aligned} f_k(\varphi,\phi,t) &:= (1-\phi)f_{\mathrm{b}}(\varphi) + \big(j_{\mathrm{b}}(\phi) - (1-\phi)q_k(t)\big)\varphi \\ &= (1-\phi)f_{\mathrm{b}}(\varphi) + \big(j_k(\phi,t) - q_k(t)\big)\varphi, \quad k = 1,2. \end{aligned}$$

Here the batch drift-flux function $j_{\mathrm{b}} = j_{\mathrm{b}}(\phi)$ is given by $j_{\mathrm{b}}(\phi) = \phi\tilde{v}(\phi)$, where the drift-flux velocity function $\tilde{v}(\phi)$ is given by

$$\tilde{v}(\phi) := \begin{cases} v_{\mathrm{term}}(1-\phi)^{n_{\mathrm{b}}} & \text{for } 0 \le \phi \le \phi_{\mathrm{c}}, \\ v_{\mathrm{term}}\dfrac{(1-\phi)^{2n_{\mathrm{S}}+1}}{(1-\phi_{\mathrm{c}})^{2n_{\mathrm{S}}+1-n_{\mathrm{b}}}} & \text{for } \phi_{\mathrm{c}} < \phi \le 1. \end{cases} \tag{4.2}$$

Here, v_{term} is the constant velocity of a single bubble in liquid and n_{b} a dimensionless constant. The expression in the first case of (4.2) is valid as long as the bubbles are not all in contact with each other. This contact is assumed to occur whenever ϕ exceeds the critical concentration ϕ_{c}. The expression in the second case of (4.2) is derived from a compatibility condition which makes it possible to express the drainage velocity of liquid in the froth relative to the bubbles with respect to gravity and dissipation in terms of v_{term} and the dimensionless constant n_{S}. The latter emerges from empirical connections between the radius of Plateau borders in the foam, the radius of the bubbles and the volume fraction of the liquid in the foam $1-\phi$; see Bürger et al. (2022) for all

details. The function $d(\phi)$ describes capillarity and is given by

$$d(\phi) := \begin{cases} 0 & \text{for } 0 \le \phi \le \phi_c, \\ v_{\text{term}} d_{\text{cap}} \dfrac{\phi(1-\phi)^{n_S}}{(1-\phi_c)^{2n_S+1-n_b}} & \text{for } \phi_c < \phi \le 1, \end{cases} \tag{4.3}$$

where d_{cap} is a capillarity-to-gravity constant present in the froth when $\phi > \phi_c$ and it involves among others the surface tension of water; see Bürger et al. (2022). For the steady states and operating charts as well as the numerical simulations in this work we utilize $\phi_c = 0.74$ (cf. Eq. (21) of Neethling and Cilliers, 2003) and $n_S = 0.46$ (Stevenson et al., 2008). In light of (4.3) we obtain

$$D(\phi) = \begin{cases} 0 & \text{for } 0 \le \phi \le \phi_c, \\ v_{\text{term}} d_{\text{cap}} \dfrac{\omega(\phi_c) - \omega(\phi)}{(1-\phi_c)^{2n_S+1-n_b}(n_S+1)(n_S+2)} & \text{for } \phi_c < \phi \le 1, \end{cases}$$

where $\omega(\phi) := (1-\phi)^{n_S+1}((n_S+1)\phi+1)$. Finally, we define the total convective flux for the solids appearing in the governing system (4.1) by

$$\tilde{F}(\psi, \phi, z, t) := \begin{cases} F(\psi/(1-\phi), \phi, z, t) & \text{for } 0 \le \phi < 1, \\ 0 & \text{for } \phi = 1. \end{cases}$$

5. Desired steady states

In the case of absence of capillarity, Bürger et al. (2019) provided detailed constructions of all steady states, and sorted out (Bürger et al. 2020a, 2020b) the most interesting steady states for the applications and how to control these by letting the volumetric flows satisfy certain nonlinear inequalities, which can be visualized in so-called operating charts. We assume that Q_F, ϕ_F, and ψ_F are given variables and that Q_U and Q_W are control variables. In the present context that does include capillarity and therefore froth drainage, we focus on the steady states for which a layer of froth in zone 2 is possible. We consider only solutions where the froth layer does not fill the entire zone 2, so that there is at least a small region above the feed inlet with aggregate volume fraction below the critical one. The wash water is sprinkled at the top of the column, which is commonly done and gives fewer steady states to analyze. A desired steady state is defined to be a stationary solution that has

$$\begin{aligned} &\text{no aggregates below the feed level} && \Rightarrow \quad \phi_U = 0, \\ &\text{no solids above the feed level} && \Rightarrow \quad \varphi_E = 0, \\ &\text{a froth layer that does not fill the entire zone 2} && \Rightarrow \quad \phi(z_F^+) < \phi_c. \end{aligned} \tag{5.1}$$

The reversed implications do not hold in the two first statements: since the bulk flow in zone 1 is directed downwards, there exist steady-state solutions with a standing layer of aggregates below the feed level, and analogously, if the bulk flow in zone 2 is directed upwards, there may be a layer of standing solids when their settling velocity is balanced by the upward bulk velocity (Bürger et al., 2019).

The construction of operating charts is detailed by Bürger et al. (2022). These are maps that indicate the regions of the (Q_U, Q_F)-plane where for given material specific functions (4.2) and (4.3) and values of ϕ_F, ψ_F, and Q_W, all algebraic inequalities that ensure that all of (5.1) hold are satisfied. Verifying satisfaction of the condition concerning the width of the froth layer requires solving (numerically) one ordinary differential equation per (Q_U, Q_F) pair. We omit any detail of the procedure here (see Bürger et al., 2022; Betancourt et al., 2023) but provide in Figure 2

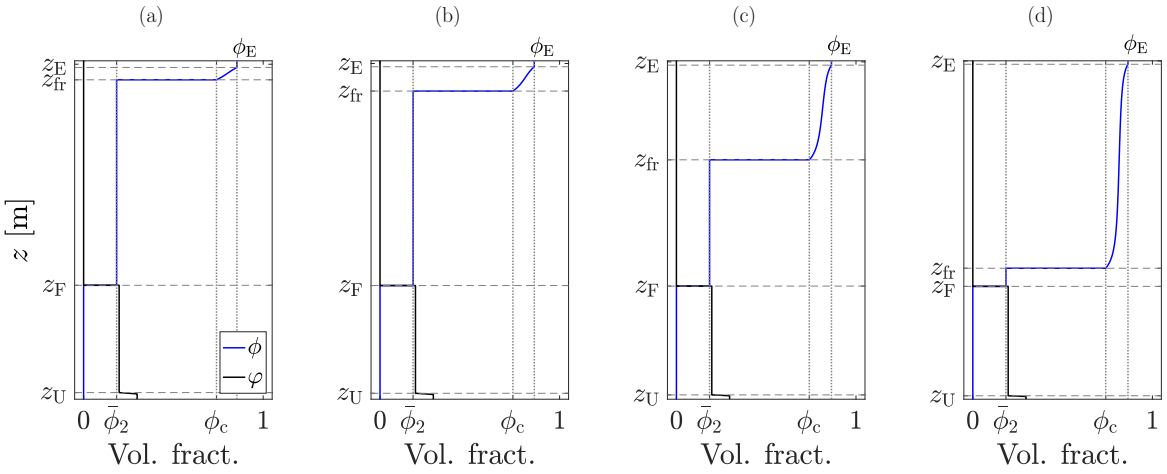

FIGURE 2. Examples of desired steady states for bubble concentration ϕ (blue) and solids concentration ψ (black) We use fixed values of $\phi_{\mathrm{F}} = 0.3$, $\psi_{\mathrm{F}} = 0.2$, $Q_{\mathrm{F}} = 8.85 \times 10^{-5}\,\mathrm{m}^3/\mathrm{s}$ and $Q_{\mathrm{W}} = 2 \times 10^{-6}\,\mathrm{m}^3/\mathrm{s}$ and vary Q_{U}, choosing: (a) $Q_{\mathrm{U}} = 5.94 \times 10^{-5}\,\mathrm{m}^3/\mathrm{s}$, (b) $Q_{\mathrm{U}} = 5.96 \times 10^{-5}\,\mathrm{m}^3/\mathrm{s}$, (c) $Q_{\mathrm{U}} = 5.975 \times 10^{-5}\,\mathrm{m}^3/\mathrm{s}$ and (d) $Q_{\mathrm{U}} = 5.977 \times 10^{-5}\,\mathrm{m}^3/\mathrm{s}$. Once the values of ϕ_{F}, Q_{U}, Q_{F} and Q_{W} are chosen, the values of the effluent concentration ϕ_{E} are given by $\phi_{\mathrm{E}} = Q_{\mathrm{F}}\phi_{\mathrm{F}}/(Q_{\mathrm{W}} + Q_{\mathrm{F}} - Q_{\mathrm{U}})$ and used as input in the steady-state ODE to calculate the value of z_{fr}. In particular, we get (a) $\phi_{\mathrm{E}} = 0.8537$, (b) $\phi_{\mathrm{E}} = 0.8592$, (c) $\phi_{\mathrm{E}} = 0.8634$ and (d) $\phi_{\mathrm{E}} = 0.8640$.

some examples of steady states, shown as ϕ- and ψ-profiles with a vertical z-axis. (The steady-state constructions, operating charts, and numerical simulations in this work are based on setting $z_{\mathrm{U}} = 0\,\mathrm{m}$, $z_{\mathrm{F}} = 0.33\,\mathrm{m}$, and $z_{\mathrm{E}} = 1\,\mathrm{m}$.) On the other hand, Figure 3 (a) is an example of an operating chart; the narrow, wedge-shaped white region indicates the choices of $(Q_{\mathrm{U}}, Q_{\mathrm{F}})$ that lead to a desirable steady state. In contrast, Figure 4 illustrates the dynamic effects of varying the parameters of the drift-flux velocity function $\tilde{v}(\phi)$, the terminal velocity v_{term}, and the dimensionless constant n_{b} on the operating charts. To systematically explore the influence of these parameters on the operating conditions, we adjusted each parameter individually while keeping the others constant. This approach allows us to isolate the effects of each parameter on the dynamics of the system. The functions $\tilde{v}(\phi)$ and $D(\phi)$ arising from this variation of n_{b} and v_{term} are plotted in Figure 5.

To understand the effects of capillarity on froth dynamics, in Figure 6 the exact solution for calculating the foam height was first computed. Subsequent modifications were made to the capillarity-to-gravity parameter d_{cap}, which was incrementally increased by 5%, 15%, and 25%. These modifications provided insight into how changes in capillary forces influence the height of the froth layer.

Operating charts showing the effects of varying the dimensionless constant n_{b} across different values of the terminal velocity v_{term}. In the first row, $v_{\mathrm{term}} = 1.6 \times 10^{-2}\,\mathrm{m/s}$ with n_{b} values of 2.0, 2.4, and 3.2. In the second row, $v_{\mathrm{term}} = 2.6 \times 10^{-2}\,\mathrm{m/s}$ and n_{b} varied as in the first row. In the third row, $v_{\mathrm{term}} = 3.6 \times 10^{-2}\,\mathrm{m/s}$, again with the same variations in n_{b}. Each chart illustrates how shifts in n_{b} and v_{term} affect the regions indicating a desirable steady state.

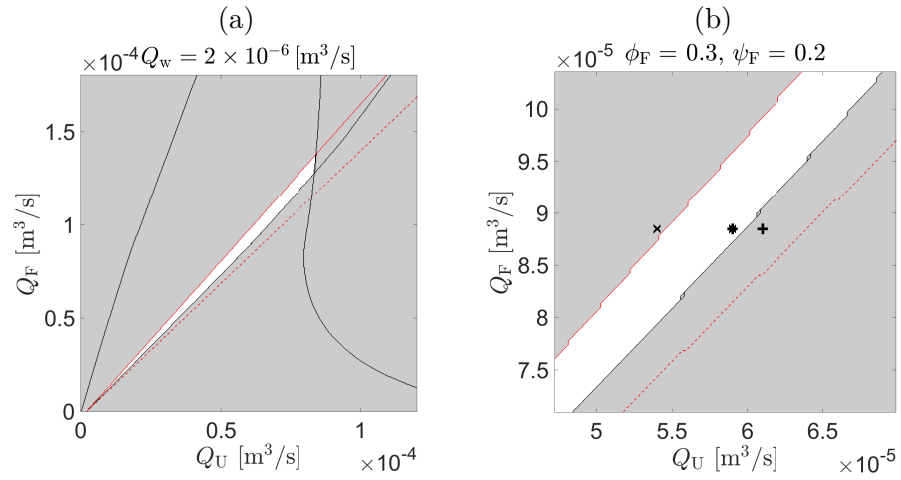

FIGURE 3. (a) Operating chart for $Q_W = 2 \times 10^{-6}\,\mathrm{m}^3/\mathrm{s}$, $\phi_F = 0.3$ and $\psi_F = 0.2$. The lines correspond to inequalities that have to be satisfied for a desired steady state. All such are satisfied in the white region, which indicates the choices of (Q_U, Q_F) that lead to a desirable steady state, (b) enlarged view of (a). The point $(Q_U, Q_F) = (5.9, 8.85) \times 10^{-5}\,\mathrm{m}^3/\mathrm{s}$ marked with a star ("$*$") in the white region results in a desired steady state with a froth layer at the top of the column. The points marked with a cross ("$\times$") $(Q_U, Q_F) = (5.4, 8.85) \times 10^{-5}\,\mathrm{m}^3/\mathrm{s}$ and a plus ("+") $(Q_U, Q_F) = (6.1, 8.85) \times 10^{-5}\,\mathrm{m}^3/\mathrm{s}$ result in no froth (Figure 7 (a) and (b)) or a tank full of froth (Figure 7 (c) and (d)), respectively.

6. NUMERICAL METHOD

The numerical method used for the solution of the complete model is outlined by Bürger et al. (2022). It is based on subdividing the computational domain (that is, the interval $[z_U, z_E]$) into a number N of layers (subintervals) of equal height Δz, and time is discretized via $t_n = n\Delta t$, $n = 0, 1, 2, \ldots$. Without entering into any details, assume that the unknowns of the scheme are ϕ_j^n and ψ_j^n, where these quantities are approximate values of ϕ and ψ in cell j at time t_n, respectively. The general scheme can then be written in the form

$$\begin{aligned} \phi_j^{n+1} &= \mathcal{H}\big(\phi_{j-1}^n, \phi_j^n, \phi_{j+1}^n, j, n\big), \\ \psi_j^{n+1} &= \mathcal{K}\big(\phi_{j-1}^n, \phi_j^n, \phi_{j+1}^n, \psi_{j-1}^n, \psi_j^n, \psi_{j+1}^n, j, n\big), \quad j = 1, \ldots, N; \quad n = 0, 1, 2, \ldots. \end{aligned} \tag{6.1}$$

The functions $\mathcal{H}$ and $\mathcal{K}$ are chosen in such a way that (6.1) represents a consistent finite difference approximation of the system (4.1) (see Bürger et al. (2022) for all details). The formulation (6.1) is useful to point out some particular properties of the numerical scheme of Bürger et al. (2022): first of all, the scheme is explicit, that is, from given initial values ϕ_j^0 and ψ_j^0, $j = 1, \ldots, N$, one calculates successively ϕ_j^1 and ψ_j^1, $j = 1, \ldots, N$, then ϕ_j^2 and ψ_j^2, $j = 1, \ldots, N$, and so on for $n = 3, 4, \ldots$. Furthermore, the system (4.1) is triangular, which means that the first equation contains apart from $\partial\phi/\partial t$ only terms that depend on known functions and ϕ and its z-derivatives. On the contrary, the second PDE, for the update of ψ, contains apart from $\partial\psi/\partial t$ terms that depend on both ϕ and ψ. Thus, the bubble volume fraction ϕ can be updated independently from the solids volume fraction ψ, which is also reflected in (6.1). The functions $\mathcal{H}$ and $\mathcal{K}$ are based on particular numerical fluxes that satisfy the so-called monotonicity property, which ensures that if

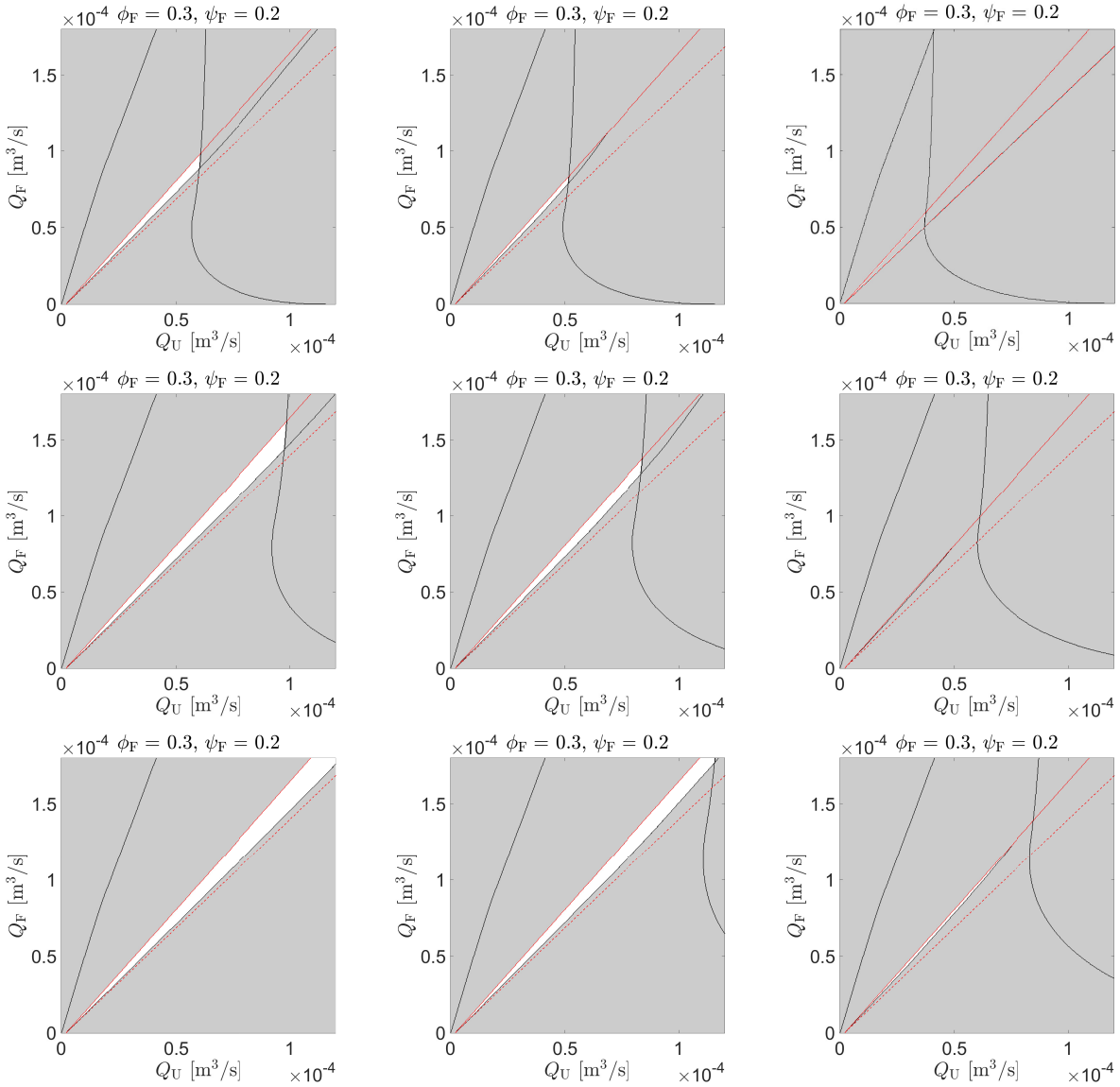

FIGURE 4. Operating charts showing the effects of varying the dimensionless constant n_b across different values of the terminal velocity v_term. In the first row, $v_\mathrm{term} = 1.6 \times 10^{-2}\,\mathrm{m/s}$ with n_b values of 2.0, 2.4, and 3.2. In the second row, $v_\mathrm{term} = 2.6 \times 10^{-2}\,\mathrm{m/s}$ and n_b varied as in the first row. In the third row, $v_\mathrm{term} = 3.6 \times 10^{-2}\,\mathrm{m/s}$, again with the same variations in n_b. Each chart illustrates how shifts in n_b and v_term affect the region indicating a desirable steady state.

the initial values are physically relevant, i.e.,

$$\phi_j^n \geq 0, \quad \psi_j^n \geq 0, \quad \phi_j^n + \psi_j^n \leq 1 \quad \text{for all } j$$

is in effect for $n = 0$, then the same property is valid for all $n = 1, 2, \ldots$. The latter property makes the approach by Bürger et al. (2022) interesting for practical applications. That said, for a given

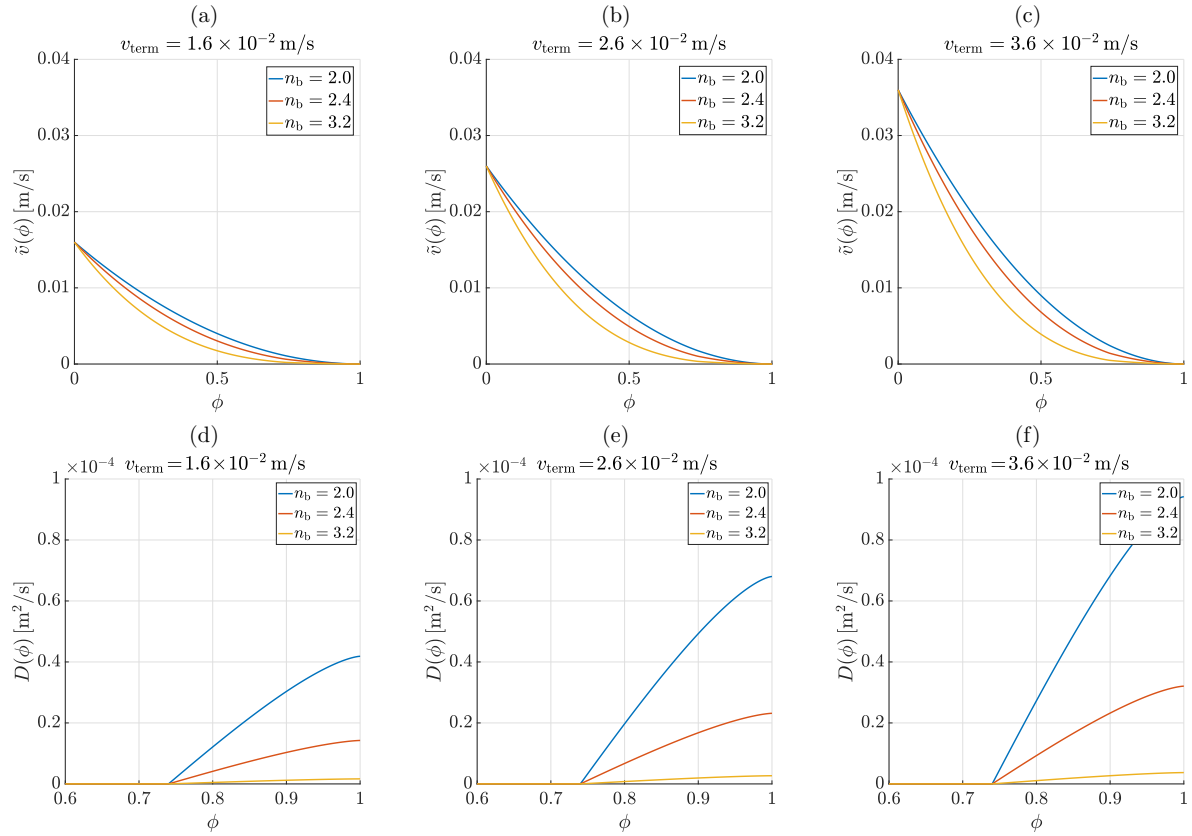

FIGURE 5. Functions (a, b, c) $\tilde{v}(\phi)$ and (d, e, f) $D(\phi)$ corresponding to the operating charts of Figure 4.

layer thickness Δz one needs to choose the time step Δt in such a way that the so-called Courant-Friedrichs-Lewy (CFL) condition is satisfied. Such a condition also ensures that the numerical approximations converge (as $\Delta z, \Delta t \to 0$) to an exact solution of the model, as is outlined by Bürger et al. (2023).

7. NUMERICAL EXAMPLE

To demonstrate that operating points outside the white region lead to non-desired steady states, we include an enlightening example similar to Example 2 of Bürger et al. (2022) but with different parameters. We start from a column filled with only water at $t = 0\,\text{s}$, i.e., $\phi(z,0) = \psi(z,0) = 0$ for all z, when we start pumping aggregates, solids, fluid and wash water with $\phi_F = 0.3$ and $\psi_F = 0.2$. In the white region of the operating chart in Figure 3 (b), we choose the point ("$*$") $(Q_U, Q_F) = (5.9, 8.85) \times 10^{-5}\,\text{m}^3/\text{s}$. The wash water volumetric flow is $Q_W = 2.0 \times 10^{-6}\,\text{m}^3/\text{s}$. Then one obtains a desired steady state with a thin layer of froth at the top and solids only below the feed level after about 800 s; see Figures 7 (a) and (c). At this time we perform two alternative different changes corresponding to the points "$\times$" and "$+$" in the operating chart in Figure 3 (b). The jump from the middle point ("$*$") to "$\times$" means a jump from $Q_U = 5.9 \times 10^{-5}\,\text{m}^3/\text{s}$ to the smaller value $5.4 \times 10^{-5}\,\text{m}^3/\text{s}$ and produces the solution in Figures 7 (a) and (b). Soon after $t = 800\,\text{s}$, the froth has been washed out upwards and the solids volume fraction is slightly higher in the new steady state. If the jump from "$*$" instead goes to "$+$", i.e., the new value at $t = 800\,\text{s}$

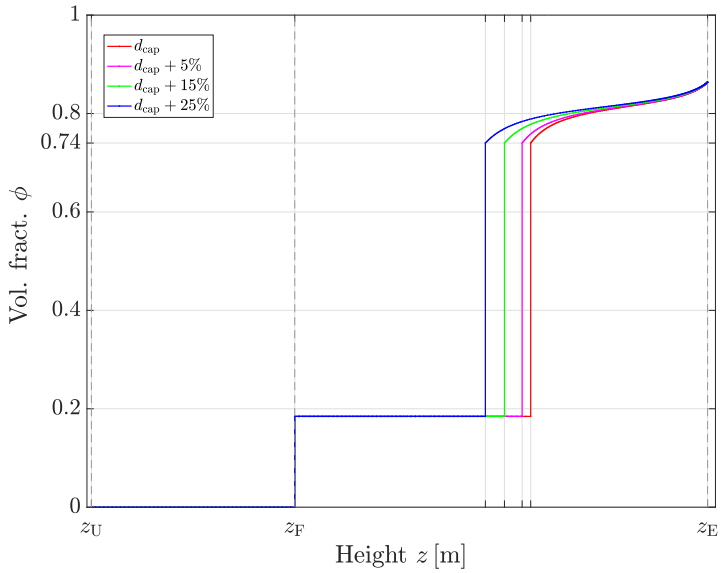

FIGURE 6. Illustration of froth height response to incremental increases in the capillarity-to-gravity parameter d_{cap}. The scenario is depicted alongside three additional scenarios where d_{cap} was increased by 5%, 15%, and 25%.

is the larger $Q_{\text{U}} = 6.1 \times 10^{-5}\,\text{m}^3/\text{s}$, Figures 7 (c) and (d) show the reaction of the system until $t = 4000\,\text{s}$. The aggregates fill the entire column while the solids volume fraction has a lower value in the new steady state.

8. Concluding remarks

The principal results of our approach have been summarized above. In light of the formulation of the model and the numerical examples, some comments on the mathematical challenges as well as limitations and future work are in place.

- The governing model is of nonlinear convection-diffusion type. Due to the nonlinearity in the convective flux and the degenerating diffusion terms, solutions are in general discontinuous. This makes a particular mathematical theory necessary.
- In addition, the governing model (4.1) involves coefficients that are discontinuous functions of the spatial coordinate z. These ingredients, and their discretization, need to be handled carefully. This is a topic of recent mathematical research; the theory is not a limiting case of equations with smooth coefficients.
- The adjustments in the drift-flux velocity function $\tilde{v}(\phi)$ and the capillarity-to-gravity parameter d_{cap} profoundly influence the dynamics of the froth layer.
- According to the results presented in Figures 4, 5, and 6, it is clear that the model is sensitive to the choice of parameters, then the techniques used in determining these will be relevant for the correct implementation and validation of the model in each particular case study.
- One of the necessary conditions for the existence of a steady state is equivalent to the well-known condition of "positive bias flow" (Dunne et al., 2019), which is the net downward

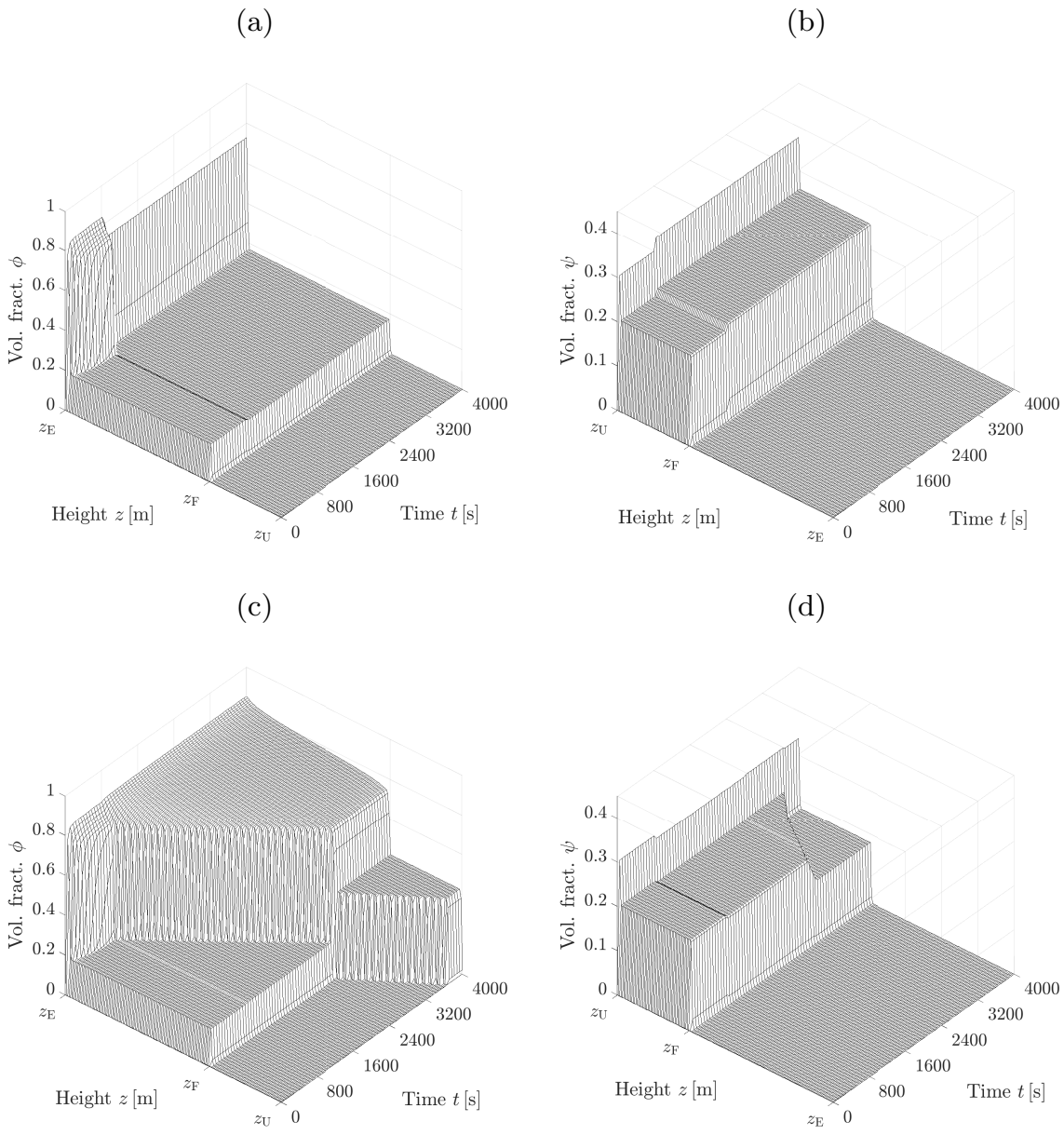

FIGURE 7. Example: Simulations with $N = 800$ of the volume fractions of (a), (c) aggregates ϕ and (b), (d) solids ψ from a tank filled with only water. (a, b) The initial operating point $(Q_{\mathrm{U}}, Q_{\mathrm{F}}) = (5.9, 8.85) \times 10^{-5}\,\mathrm{m}^3/\mathrm{s}$ ("$*$" in Figure 3 (b)) is at $t = 800\,\mathrm{s}$ changed to $(5.4, 8.85) \times 10^{-5}\,\mathrm{m}^3/\mathrm{s}$ ("$\times$" in Figure 3 (b)). (c, d) The initial operating point $(Q_{\mathrm{U}}, Q_{\mathrm{F}}) = (5.9, 8.85) \times 10^{-5}\,\mathrm{m}^3/\mathrm{s}$ is at $t = 800\,\mathrm{s}$ changed to $(6.1, 8.85) \times 10^{-5}\,\mathrm{m}^3/\mathrm{s}$ ("$+$" in Figure 3 (b)). Note the reversed z-axes for aggregates and solids.

flow of water through zone 2. A proper formulation of this observation and its consequences is being investigated.

- The model variant with separated gas and pulp inlets includes a collection zone. We are currently modeling the adhesion of hydrophobic particles to bubble surfaces to describe this phenomenon.

Acknowledgements

The authors' research, and its presentation at Flotation '23, are funded by ANID (Chile) projects Fondecyt 1210610 (to R.B., M.C.M. and Y.V.); Anillo ANID/ACT210030 (to F.B., R.B., M.C.M. and Y.V.), Centro de Modelamiento Matemático (CMM), project FB210005 of BASAL funds for Centers of Excellence (to F.B. and R.B.); and CRHIAM, projects ANID/FONDAP/15130015 and ANID/FONDAP/1523A0001 (to F.B. and R.B.). In addition, S.D. acknowledges support from the Swedish Research Council (Vetenskapsrådet, 2019-04601); M.C.M. is supported by grant PID2020-117211GB-I00 funded by MCIN/AEI/10.13039/501100011033 and project CIAICO/2021/227; and Y.V. is supported by Centro de Estudios Multidisciplinarios en Ciencias, Ingeniería y Tecnología AIP (CEMCIT AIP, Panama).

References

Azhin, M., Popli, K., Afacan, A., Liu, Q., Prasad, V., 2021a. A dynamic framework for a three phase hybrid flotation column. Minerals Eng. 170, article 107028.

Azhin, M., Popli, K., Prasad, V., 2021b. Modelling and boundary optimal control design of hybrid column flotation. Canad. J. Chem. Eng. 99, S369–S388.

Bergh, L. G., Yianatos, J. B., 2022. The long way to multivariate predictive control of flotation processes. J. Process Control 21, 226–234.

Betancourt, F., Bürger, R., Diehl, S., Gutiérrez, L., Martí, M. C., Vásquez, Y., 2023. A model of froth flotation with drainage: Simulations and comparison with experiments. Minerals 13, article 344.

Brito-Parada, P. R., Neethling, S. J., Cilliers, J. J., 2012. The advantages of using mesh adaptivity when modelling the drainage of liquid in froths. Minerals Eng. 33, 80–86.

Bürger, R., Diehl, S., Martí, M. C., 2019. A system of conservation laws with discontinuous flux modelling flotation with sedimentation. IMA J. Appl. Math. 84, 930–973.

Bürger, R., Diehl, S., Martí, M. C., Vásquez, Y., 2020a. Flotation with sedimentation: Steady states and numerical simulation of transient operation. Minerals Eng. 157, article 106419.

Bürger, R., Diehl, S., Martí, M. C., Vásquez, Y., 2020b. Simulation and control of dissolved air flotation and column froth flotation with simultaneous sedimentation. Water Sci. Tech. 81, 1723–1732.

Bürger, R., Diehl, S., Martí, M. C., Vásquez, Y., 2022. A degenerating convection-diffusion system modelling froth flotation with drainage. IMA J. Appl. Math. 87, 1151–1190.

Bürger, R., Diehl, S., Martí, M. C., Vásquez, Y., 2023. A difference scheme for a triangular system of conservation laws with discontinuous flux modeling three-phase flows. Netw. Heterog. Media 18, 140–190.

Bürger, R., Karlsen, K. H., Risebro, N. H., Towers, J. D., 2004. Well-posedness in BV_t and convergence of a difference scheme for continuous sedimentation in ideal clarifier-thickener units. Numer. Math. 97, 25–65.

Bürger, R., Karlsen, K. H., Towers, J. D., 2005. A model of continuous sedimentation of flocculated suspensions in clarifier-thickener units. SIAM J. Appl. Math. 65, 882–940.

Concha A., F., Bascur, O. A., 2024. The Engineering Science of Mineral Processing. A Fundamental and Practical Approach, CRC Press, Boca Raton, FL, USA, 2024.

Cruz, E. B., 1997. A Comprehensive Dynamic Model of the Column Flotation Unit Operation. PhD thesis, Virginia Tech, Blacksburg, Virginia, USA.

Dickinson, J. E., Galvin, K. P., 2014. Fluidized bed desliming in fine particle flotation, Part I, Chem. Eng. Sci. 108, 283–298.

Diehl, S., 1996. A conservation law with point source and discontinuous flux function modelling continuous sedimentation. SIAM J. Appl. Math. 56, 388–419.

Diehl, S., 2001. Operating charts for continuous sedimentation I: control of steady states. J. Eng. Math. 41, 117–144.

Diehl, S., 2008. The solids-flux theory – confirmation and extension by using partial differential equations. Water Res. 42, 4976–4988.

Dunne, R. C., Kawatra, S. K., Young, C. A., 2019. SME Mineral Processing & Extractive Metallurgy Handbook, Society for Mining, Metallurgy, and Exploration, Englewood, CO, USA.

Ekama, G. A., Marais, P., 2004. Assessing the applicability of the 1D flux theory to full-scale secondary settling tank design with a 2D hydrodynamic model. Water Res. 38, 495–506.

Finch, J. A., Dobby, G. S., 1990. Column Flotation, Pergamon Press, London, UK.

Galvin, K. P., Dickinson, J. E., 2014. Fluidized bed desliming in fine particle flotation Part II: Flotation of a model feed. Chem. Eng. Sci. 108, 299–309.

Galvin, K.P., Harvey, N. G., Dickinson, J. E., 2014. Fluidized bed desliming in fine particle flotation – Part III flotation of difficult to clean coal. Minerals Eng. 66-68, 94–101.

Kynch, G.J., 1952. A theory of sedimentation. Transactions of the Faraday Society 48, 166–176.

Maldonado, M., Desbiens, A., del Villar, R., 2009. Potential use of model predictive control for optimizing the column flotation process. Int. J. Mineral Process. 93, 26–33.

Neethling, S. J., Brito-Parada, P. R., 2018. Predicting flotation behaviour – The interaction between froth stability and performance. Minerals Eng. 120, 60–65.

Neethling, S. J., Cilliers, J. J., 2003. Modelling flotation froths. Int. J. Mineral Process. 72, 267–287.

Neethling, S. J., Lee, H. T., Cilliers, J. J., 2002. A foam drainage equation generalized for all liquid contents, J. Physics: Condensed Matter 14, 331–342.

Pal, R., Masliyah, J. H., 1989. Flow characterization of a flotation column. Canad. J. Chem. Eng. 67, 916–923.

Quintanilla, P., Neethling, S. J., Brito-Parada, P. R., 2021a. Modelling for froth flotation control: A review. Minerals Eng. 162, article 106718.

Quintanilla, P., Neethling, S. J., Navia, D., Brito-Parada, P. R., 2021b. A dynamic flotation model for predictive control incorporating froth physics. Part I: Model development. Minerals Eng. 173, article 107192.

Quintanilla, P., Neethling, S. J., Mesa, D., Navia, D., Brito-Parada, P. R., 2021c. A dynamic flotation model for predictive control incorporating froth physics. Part II: Model calibration and validation. Minerals Eng. 173, article 107190.

Richardson, J. F., Zaki, W. N., 1954. Sedimentation and fluidisation: Part I. Trans. Inst. Chem. Engrs. (London) 32, 35–53.

Stevenson, P., 2006. Dimensional analysis of foam drainage. Chem. Eng. Sci. 61, 4503–4510.

Stevenson, P., Fennell, P. S., Galvin, K. P., 2008. On the drift-flux analysis of flotation and foam fractionation processes, Canad. J. Chem. Eng. 86, 635–642.

Tian, Y., Azhin, M., Luan, X., Liu, F., Dubljevic, S., 2018a. Three-phases dynamic modelling of column flotation process. IFAC-PapersOnLine 51 (21), 99–104.

Tian, Y., Luan, X., Liu, F., Dubljevic, S., 2018b. Y. Tian, X. Luan, F. Liu, S. Dubljevic, Model predictive control of mineral column flotation process. Mathematics 6, article 100.

Vandenberghe, J., Chung, J., Xu, Z., Masliyah, J., 2005. Drift flux modelling for a two-phase system in a flotation column. Canad. J. Chem. Eng. 83, 169–176.

Vásquez, Y., 2022. Conservation Laws with Discontinuous Flux Modeling Flotation Columns. Doctoral Thesis, Universidad de Concepción, Concepción, Chile.

Wallis, G. B., 1969. One-Dimensional Two-Phase Flow, McGraw-Hill, New York.

Wang, G., Ge, L., Mitra, S., Evans, G. M., Joshi, J. B., Chen, S., 2018. A review of CFD modelling studies on the flotation process. Minerals Eng. 127, 153–177.

Wills, B. A., Napier-Munn, T. (Eds.), 2006. Wills' Mineral Processing Technology. Seventh Edition. Butterworth-Heinemann/Elsevier, Oxford, UK.

Centro de Investigación en Ingeniería Matemática (CI^{2}MA)

PRE-PUBLICACIONES 2023 - 2024

2023-28 Marie Haghebaert, Beatrice Laroche, Mauricio Sepúlveda: *Study of the numerical method for an inverse problem of a simplified intestinal crypt*

2023-29 Rodolfo Araya, Fabrice Jaillet, Diego Paredes, Frederic Valentin: *Generalizing the Multiscale Hybrid-Mixed Method for Reactive-Advective-Diffusive Equations*

2023-30 Jessika Camaño, Ricardo Oyarzúa, Miguel Serón, Manuel Solano: *A mass conservative finite element method for a nonisothermal Navier-Stokes/Darcy coupled system*

2023-31 Franz Chouly, Hao Huang, Nicolás Pignet: *HHT-α and TR-BDF2 schemes for Nitsche-based discrete dynamic contact*

2024-01 Sergio Caucao, Gabriel N. Gatica, Saulo Medrado, Yuri D. Sobral: *Nonlinear twofold saddle point-based mixed finite element methods for a regularized $\mu(I)$-rheology model of granular materials*

2024-02 Julio Careaga, Gabriel N. Gatica, Cristian Inzunza, Ricardo Ruiz-Baier: *New Banach spaces-based mixed finite element methods for the coupled poroelasticity and heat equations*

2024-03 Harold D. Contreras, Paola Goatin, Luis M. Villada: *A two-lane bidirectional nonlocal traffic model*

2024-04 Rommel Bustinza, Matteo Cicuttin, Ariel Lombardi: *A Hybrid High-Order method for the mixed Steklov eigenvalue problem*

2024-05 Isaac Bermudez, Jaime Manríquez, Manuel Solano: *A hybridizable discontinuous Galerkin method for Stokes/Darcy coupling in dissimilar meshes*

2024-06 Thomas Führer, Diego Paredes: *Robust hybrid finite element methods for reaction-dominated diffusion problems*

2024-07 Raimund Bürger, Enrique D. Fernández Nieto, Jorge Moya: *A multilayer shallow water model for tsunamis and coastal forest interaction*

2024-08 Fernando Betancourt, Raimund Bürger, Stefan Diehl, María Carmen Martí, Yolanda Vásquez: *A degenerating convection-diffusion model of a flotation column: theory, numerics and applications*

Para obtener copias de las Pre-Publicaciones, escribir o llamar a: Director, Centro de Investigación en Ingeniería Matemática, Universidad de Concepción, Casilla 160-C, Concepción, Chile, Tel.: 41-2661324, o bien, visitar la página web del centro: http://www.ci2ma.udec.cl







Centro de Investigación en
Ingeniería Matemática (CI²MA)
Universidad de Concepción

Casilla 160-C, Concepción, Chile
Tel.: 56-41-2661324/2661554/2661316
http://www.ci2ma.udec.cl